# Communication

## A Wideband 2-D Fast Multipole Algorithm With a Novel Diagonalization Form

Ling Ling Meng, Mert Hidayetoğlu, Tian Xia, Wei E. I. Sha, Li Jun Jiang, and Weng Cho Chew

***Abstract*— It is well known that Green's function can be expressed by multipole expansion, plane-wave expansion, and exponential expansion (spectral representation). These three expansions constitute of the foundations of the fast multipole algorithm (FMA). The plane-wave expansion has the low-frequency breakdown issue due to its failure in capturing the evanescent spectra, while the multipole expansion is inefficient at high frequencies. The spectral representation usually involves in direction-dependent issue. In this communication, the 2-D FMA is interpreted as Parseval's theorem in Fourier transform. To achieve a stable and accurate transition between the multipole expansion and the plane-wave expansion, a novel diagonalization in the 2-D FMA is proposed with scaled special functions based on a discrete Fourier transform. A wideband fast algorithm with high accuracies can be achieved efficiently.**

***Index Terms*— Discrete Fourier transform (DFT), multipole expansion, Parseval's theorem, plane-wave expansion.**

### I. Introduction

The fast multipole algorithm (FMA) has been proposed for two decades because of its initial version for solving coulombic interactions in large-scale particle problems [1], [2]. A lot of research has made contributions to the study in FMA, among which the multilevel FMA with interpolation and anterpolation is the most adopted one [3], [4], which is extended to mixed-form FMA and applied to dielectric problems [5], [6]. It can be used to solve the problems of three billion unknowns with the advancements in parallel computer hardware and efficient implementations [7]. Less attention is paid to 2-D FMA since it is easier, less complicated, and even less applicable to real situations than the 3-D counterpart. A normalized plane-wave method for 2-D Helmholtz problems has been proposed for a wideband algorithm [8]. Recent studies in devices with dielectric materials and imaging with inverse scattering problems require a fast and efficient algorithm for inhomogeneous media. The 2-D FMA with the plane-wave expansion has been successfully incorporated for fast full-wave tomographic image reconstruction, where the Helmholtz equation is solved without any wave approximation [9]. However, these implementations suffer from the low-frequency breakdown and therefore cannot be employed for many ultrasound and seismic imaging methods where the incident wave is a pulse with a wide bandwidth. Therefore, a scalable, wideband FMA solver is highly desirable for real-world imaging applications. Besides, the study of the 2-D FMA provides insights for the solutions to the 3-D case, as they share the same physics.

The addition theorem of Green's function can be interpreted as Parseval's theorem in Fourier transform for 2-D cases [4]. This naturally leads to the two forms of FMA, i.e., multipole expansion in coordinate space and plane-wave expansion in Fourier space. Then, the diagonalization of FMA from a dense matrix in the multipole expansion to a diagonal matrix in the plane-wave expansion can be taken as the transformation of a convolution in coordinate space to an ordinary multiplication in Fourier space, which reduces the computational complexity greatly. The plane-wave expansion has the low-frequency breakdown issue due to its failure in capturing the evanescent spectra. Mathematically, it is because of a finite summation of Hankel functions with super large values when the argument is close to the singularity point. Meanwhile, the multipole expansion is inefficient at high frequency since higher order multipoles are required, which brings in an impractical cost in the computation of dense matrices. Similar scenarios exist in the 3-D case. A broadband 3-D FMA can be achieved by the enhanced mixed-form FMA with rotation matrices in high-order multipoles [5] or by the approximated diagonalization of Green's function with a normalization technique [10], [11]. The spectral representation of Green's function can also achieve a broadband scheme by expressing the fields with both propagating and evanescent parts explicitly. To find an efficient integral path in spectral representation, it introduces direction-dependence issue (six directions have to be considered) that requires other techniques (such as rotation [12] and QR decomposition-algorithm [13]) or more memory storage and operations in an FMA procedure [14].

In this communication, we focus on the 2-D case due to its potential applications mentioned before. Besides, we prefer not to introduce the direction-dependence issue; therefore, the spectral representation in the 2-D case is not considered here. To remedy the gap between them, a novel diagonalization is proposed in this communication based on the aforementioned idea of Fourier transform with scaled special functions. This is different from the derivations in [8], which inserted identities of Kronecker delta function. To clarify the novelty of this communication, it is noted that the proposed idea to achieve a broadband FMA is essentially different from the work [10] (in which the approximated formula of Bessel functions is used), though both of them use the normalization technique. The translators in multipole expansions are set up as a set of Fourier coefficients with a scaling parameter, and therefore, there is no dense matrix anymore. Then, the subsequent aggregation, translation, and disaggregation are calculated in Fourier space. Since the Hankel functions have been normalized, the breakdown issue is overcome in the gap region with comparable complexity in the plane-wave expansion. The rest of this communication is organized as follows. Section II gives the derivation of this novel diagonalization and the numerical treatments. In Section III, numerical analysis is provided.

Manuscript received December 24, 2017; revised June 27, 2018; accepted August 23, 2018. Date of publication September 26, 2018; date of current version November 30, 2018. This work was supported in part by the NCSA Petascale Application Improvement Discovery Program and in part by NSF under Grant EECS 1609195. *(Corresponding author: Weng Cho Chew.)*

L. L. Meng, M. Hidayetoğlu, and T. Xia are with the Department of Electrical and Computer Engineering, University of Illinois of Urbana–Champaign, Urbana, IL 61820 USA (e-mail: lmeng9@illinois.edu; hidayet2@illinois.edu; tianxia3@illinois.edu).

W. E. I. Sha is with the College of Information Science and Electronic Engineering, Zhejiang University, Hangzhou 310027, China (e-mail: weisha@zju.edu.cn).

L. J. Jiang is with the Department of Electrical and Electronic Engineering, The University of Hong Kong, Hong Kong (e-mail: jianglj@hku.hk).

W. C. Chew is with the Department of Electrical and Computer Engineering, Purdue University, West Lafayette, IN 47907 USA (e-mail: wcchew@purdue.edu).

Color versions of one or more of the figures in this communication are available online at http://ieeexplore.ieee.org.

Digital Object Identifier 10.1109/TAP.2018.2872167

The proposed broadband FMA is applied to the volume integral equation (VIE) [15] to study the scattering of dielectric cylinders in 2-D photonic crystals. The analysis of defect modes serves as the applications in low-frequency regime. On the other hand, the study of wave propagation in photonic crystal waveguides plays a role in the applications for high-frequency regime. Section IV concludes the algorithm and discusses its extensions for the 3-D case.

## II. Theory of Combined-Form Fast Multipole Algorithm

In this section, the conventional diagonalization in 2-D FMA is briefly introduced based on the interpretation of Parseval's theorem. Then, the discrete Fourier transform (DFT) FMA is proposed with scaled special functions. Afterward, its extension to multilevel structures and conversion to the plane-wave expansion are given.

### A. Parseval's Theorem and Diagonalization in FMA

According to the addition theorem, the factorization of Green's function has the following multipole expansion [4], if $\boldsymbol{\rho}_{ji} = \boldsymbol{\rho}_{jl'} + \boldsymbol{\rho}_{l'l} + \boldsymbol{\rho}_{li}$:

$$H_0^{(1)}(k\rho_{ji}) = \sum_{m=-\infty}^{+\infty} a_m^* \cdot \sum_{n=-\infty}^{+\infty} H_{m-n}^{(1)}(k\rho_{l'l})e^{-i(m-n)\phi_{l'l}}d_n \tag{1}$$

where

$$a_m = J_m(k\rho_{jl'})e^{-im(\phi_{jl'}-\pi)} \tag{2}$$

and

$$d_n = J_n(k\rho_{li})e^{-in(\phi_{li})}. \tag{3}$$

The radiation pattern $\{d_n\}$ and the receiving pattern $\{a_m\}$ in the multipole expansion are the Fourier coefficients with $e^{in(\phi-\pi/2)}$ bases. The corresponding Fourier series are

$$e^{-ik\rho_{li}\cos(\phi-\phi_{li})} = e^{-i\mathbf{k}\cdot\boldsymbol{\rho}_{li}} = \sum_{n=-\infty}^{+\infty} d_n e^{in(\phi-\pi/2)} \tag{4}$$

and

$$e^{ik\rho_{jl'}\cos(\phi-\phi_{jl'})} = e^{i\mathbf{k}\cdot\boldsymbol{\rho}_{jl'}} = \sum_{m=-\infty}^{+\infty} a_m e^{im(\phi-\pi/2)} \tag{5}$$

which are actually the radiation pattern and receiving pattern in the plane-wave expansion. The inner summation over $n$ of (1) is a convolution, which is a product in Fourier space. The periodic function associated with Hankel functions in a Fourier series form can be expressed as

$$\begin{aligned}\alpha(\phi) &= H_n^{(1)}(k\rho_{l'l})e^{-in\phi_{l'l}}e^{in(\phi-\pi/2)}\\ &= \sum_{n=-\infty}^{+\infty} c_n e^{in(\phi-\pi/2)}.\end{aligned} \tag{6}$$

Invoking Parseval's theorem to (1), we can write Green's function as

$$H_0^{(1)}(k\rho_{ji}) = \sum_{m=-\infty}^{+\infty} a_m^* b_m \tag{7}$$

$$= \sum_{m=-\infty}^{+\infty} a_m^* \left(\sum_{n=-\infty}^{+\infty} c_{m-n}d_n\right) \tag{8}$$

$$= \frac{1}{2\pi}\int_0^{2\pi} d\phi \left[e^{i\mathbf{k}\cdot\boldsymbol{\rho}_{jl'}}\right]^* \alpha(\phi)e^{-i\mathbf{k}\cdot\boldsymbol{\rho}_{li}} \tag{9}$$

$$= \frac{1}{2\pi}\int_0^{2\pi} d\phi\, e^{-i\mathbf{k}\cdot\boldsymbol{\rho}_{jl'}}\tilde{\alpha}(\phi)e^{-i\mathbf{k}\cdot\boldsymbol{\rho}_{li}} \tag{10}$$

where

$$\tilde{\alpha}(\phi) = \sum_{n=-P}^{+P} H_n^{(1)}(k\rho_{l'l})e^{-in(\phi_{l'l}-\phi+\pi/2)}. \tag{11}$$

Equation (10) is also named plane-wave expansions of Green's function, which is based on diagonal matrix calculations.

### B. Diagonalization With Scaled Special Functions

Although the diagonalization of the multipole expansion reduces the computation cost greatly (from dense matrices to diagonal matrices), the plane-wave expansion has the low-frequency breakdown issue. This can be explained from two factors in mathematics. One is the summation in $\tilde{\alpha}(\phi)$ [see (11)] that is divergent due to the singular property of the Hankel function for small arguments. The other one is the inaccuracy of extracting super small values from exponential functions (as the radiation pattern in the plane-wave expansion) because of machine precision. The normalization technique can be applied to scale the Hankel function. However, if we normalize those Fourier coefficients, the analytical relation of Fourier pairs is not approachable. We can use DFT to calculate the periodic functions in Fourier space numerically. We modify $a_m$, $c_n$, and $d_n$ to standard form, i.e.,

$$a'_m = J_m(k\rho_{jl'})e^{-im(\phi_{jl'}-\pi)}e^{-im\pi/2} \tag{12}$$

$$c'_n = H_n^{(1)}(k\rho_{l'l})e^{-in\phi_{l'l}}e^{-in\pi/2} \tag{13}$$

and

$$d'_n = J_n(k\rho_{li})e^{-in(\phi_{li})}e^{-in\pi/2}. \tag{14}$$

Furthermore, we split the normalization into two parts based on the sign of the subscripts of the Hankel functions. It is easier to see the cancellation of the normalization from the multipole expansion of Green's function

$$\begin{aligned}H_0^{(1)}(k\rho_{ji}) = &\sum_{m=-P}^{m=P} a_m t^{-m} \sum_{n=m-P}^{m+P} c_{m-n,m\geq n}t^{m-n}d_n t^{+n}\\ &+ \sum_{m=-P}^{m=P} a_m t^{+m}\sum_{n=m-P}^{m+P} c_{m-n,m<n}t^{n-m}d_n t^{-n}\end{aligned} \tag{15}$$

where $t$ is the normalization factor ($0 < t \leq 1$). The value of $t$ is determined according to the asymptotic form of the Hankel function and its maximum value for a certain argument as $t = (C_{max}/|H_P|)^{1/P}$, where $C_{max}$ is a preset constant, used to confine the maximum magnitude of the Hankel function within the range $0 \sim C_{max}$. For instance, $C_{max}$ can be set as $1.0E2$; then, the magnitude values of all the normalized Hankel functions are smaller than $1.0E2$, eliminating those extremely large values in unnormalized Hankel functions.

To apply DFT, the normalized Fourier coefficients for the positive part are

$$\hat{a}_m^+ = a'_m t^{-m} = J_m(k\rho_{jl'})e^{-im(\phi_{jl'}-\pi)}e^{-im\pi/2}t^{-m} \tag{16}$$

$$\hat{d}_n^+ = d'_n t^{+n} = J_n(k\rho_{li})e^{-in(\phi_{li})}e^{-in\pi/2}t^{+n} \tag{17}$$

$$\hat{c}_{n,n\geq 0}^+ = \begin{cases} H_n^{(1)}(k\rho_{l'l})e^{-in\phi_{l'l}}e^{-in\pi/2}t^{+n}, & n \geq 0\\ 0, & n < 0.\end{cases} \tag{18}$$

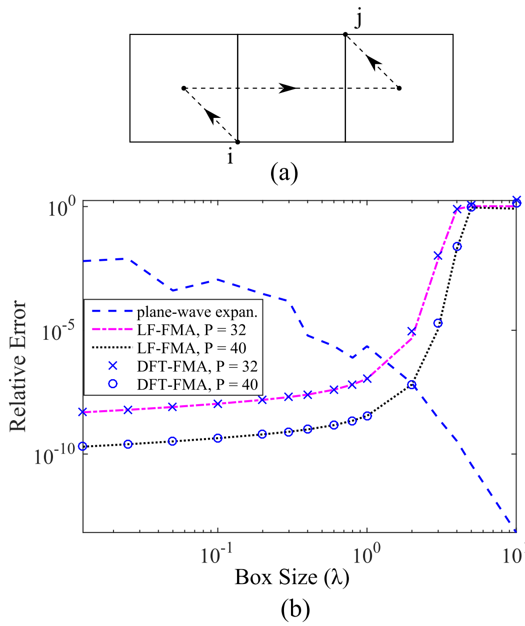


Fig. 1. (a) Configuration of the test for a set of point-to-point. (b) Error comparisons for the one-level multipole expansion, DFT-FMA, and plane-wave expansion.

For the negative part, we have

$$\hat{a}_m^- = a'_m t^{+m} = J_m(k\rho_{jl'}) e^{-im(\phi_{jl'}-\pi)} e^{-im\pi/2} t^{+m} \tag{19}$$

$$\hat{d}_n^- = d'_n t^{-n} = J_n(k\rho_{li}) e^{-in(\phi_{li})} e^{-in\pi/2} t^{-n} \tag{20}$$

$$\hat{c}_{n,n<0}^- = \begin{cases} 0, & n \geq 0 \\ H_n^{(1)}(k\rho_{l'l}) e^{-in\phi_{l'l}} e^{-in\pi/2} t^{-n}, & n < 0. \end{cases} \tag{21}$$

Now, we can write the diagonalization of normalized multipole expansions as

$$H_0^{(1)}(k\rho_{ji}) = \frac{1}{2\pi}\int_0^{2\pi} d\phi \mathcal{F}[\hat{a}_m^+]^* \mathcal{F}[\hat{c}_{n,n\geq 0}^+]\mathcal{F}[\hat{d}_n^+] + \frac{1}{2\pi}\int_0^{2\pi} d\phi \mathcal{F}[\hat{a}_m^-]^* \mathcal{F}[\hat{c}_{n,n<0}^-]\mathcal{F}[\hat{d}_n^-] \tag{22}$$

where $\mathcal{F}$ denotes the DFT. In implementation, we can use fast Fourier transform (FFT) to accelerate the algorithm further.

### *C. Scheme for Wideband Algorithm*

The DFT-FMA has the same complexity as the plane-wave expansion. It is stable at low frequency where the plane-wave expansion fails. Error analysis for one-level multipole expansion (named low frequency (LF)-FMA in convention), DFT-FMA, and plane-wave expansion can be found in Fig. 1(b) where the worst case is studied [radiation and receiving points are the diagonal vertexes of the buffer box as Fig. 1(a) shows].

The multilevel scheme makes the algorithm as a fast solver. Since the singular property of the Hankel function is rather sensitive to the argument in low-frequency regime, different normalization factors should be used at each level. For one matrix-vector product (MVP) operation, the radiation patterns start as unnormalized Fourier coefficients. During the process of aggregation, those Fourier coefficients from the children level are normalized in both negative and positive forms and then shifted with negative and positive outer-to-outer (o2o) translators. Then, the renormalization is applied to the aggregated radiation pattern, making them as unnormalized Fourier coefficients in the parent level.

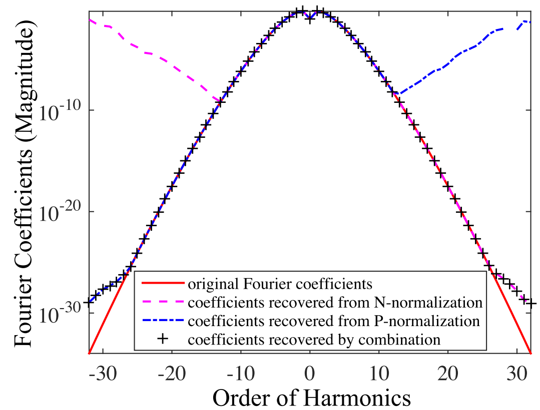


Fig. 2. Comparison of the Fourier coefficients recovered from DFT-FMA.

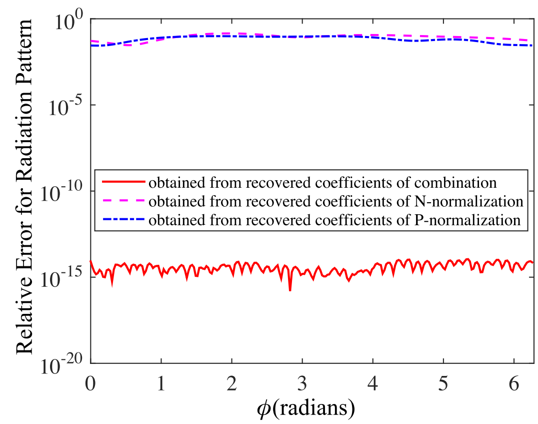


Fig. 3. Relative error of radiation pattern generated from the recovered coefficients in Fourier space.

Ideally, the set of Fourier coefficients recovered from the negative normalization should be equal to the set from the positive one. However, due to the finite machine precision, the renormalization introduces errors (see Fig. 2).

The accurate recovered coefficients can be obtained by combining the left half from the positive normalization and the right half from the negative normalization (see the black cross line in Fig. 2). Assuming that $\{u_n\}$ is the set of Fourier coefficients in the parent level, then, the o2o translation can be expressed as the following compact form:

$$\{u_n\} = [\bar{S}] \cdot \{t^{-n}\} \cdot [\bar{F}]^{-1} \cdot \tilde{\bar{\beta}}^+ \cdot [\bar{F}] \cdot \{d'_n t^{+n}\} + [\bar{I} - \bar{S}] \cdot \{t^{+n}\} \cdot [\bar{F}]^{-1} \cdot \tilde{\bar{\beta}}^- \cdot [\bar{F}] \cdot \{d'_n t^{-n}\} \tag{23}$$

where $[\bar{F}]$ and $[\bar{F}]^{-1}$ denote the operations of Fourier transform and inverse Fourier transform, respectively. Symbolic matrices $[\bar{S}]$ and $[\bar{I} - \bar{S}]$ represent the manipulation of taking the proper half parts from the negative and positive renormalized coefficients.

A similar process happens during the outer-to-inner translation in the DFT-FMA. When the ratio of box size over the wavelength at a certain level enters the middle-frequency regime (for instance, the ratio of 2.0 in Fig. 1), no normalization is required, since the plane-wave expansion works very well. Then, the stored Fourier coefficients are transformed to the plane-wave form followed by the o2o shifting. Fig. 3 shows the relative error of the radiation pattern generated from the combined coefficients, recovered coefficients only from the negative normalization, and recovered coefficients only from

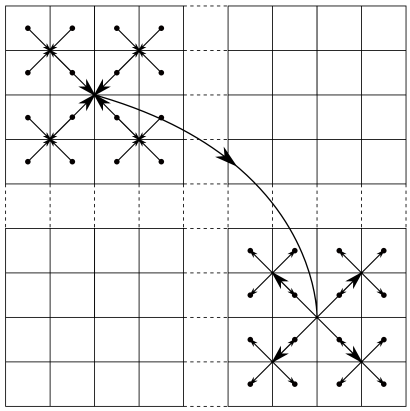

Fig. 4. Multilevel structure (partial points shown).

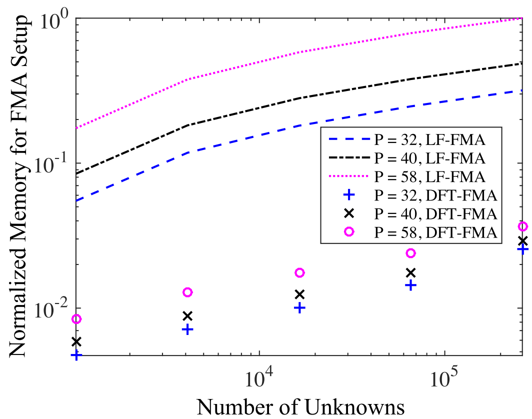


Fig. 5. Normalized memory for FMA setup in the LF-FMA and the DFT-FMA.

the positive normalization in reference to the analytical plane-wave expression. It can be found that the conversion from the DFT-FMA to the plane-wave expansion is of high accuracy.

It should be noted that the disaggregation part is the transpose conjugate of the aggregation part, and thus, we can arrive at a wideband multilevel algorithm with high accuracies.

## III. Numerical Results

Numerical analyses of the pure DFT-FMA and the aforementioned FMA with a combination of different forms (denoted as Comb-form-FMA, in which the DFT-FMA serves in the transition region between the multipole expansion and the plane-wave expansion) are given in this section. Then, this new wideband fast technique is applied to the VIE to solve the scattering problems of dielectric cylinders in 2-D photonic crystals.

### A. Complexities and Error Analysis of DFT-FMA

First, we compare the performance of the DFT-FMA with the multipole expansion by changing the number of levels when the leaf box size is fixed (this changes the number of unknowns). The source points and field points are distributed on each grid of the whole domain. A simple illustration of the multilevel structure is given in Fig. 4, where only partial points are shown. Figs. 5 and 6 show the normalized memory cost and time cost for the FMA setup with the number of harmonics of 32, 40, and 58. It can be seen that the DFT-FMA reduces both the memory and time cost greatly. The Larger number of harmonics results in larger difference. The normalized

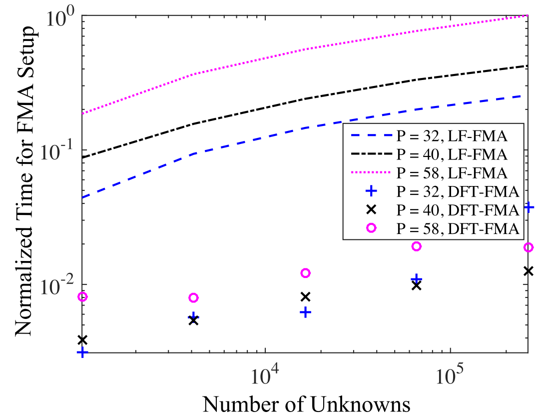


Fig. 6. Normalized time cost for FMA setup in the LF-FMA and the DFT-FMA.

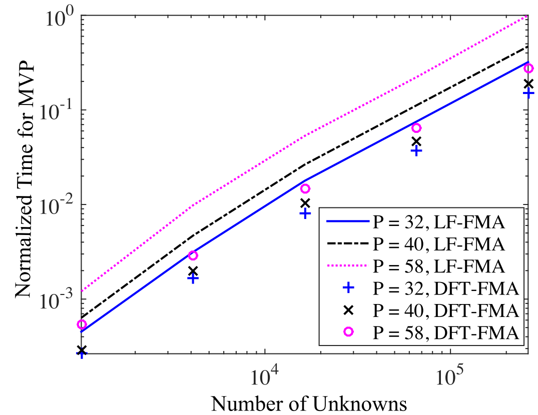


Fig. 7. Normalized time cost for MVP in the LF-FMA and the DFT-FMA.

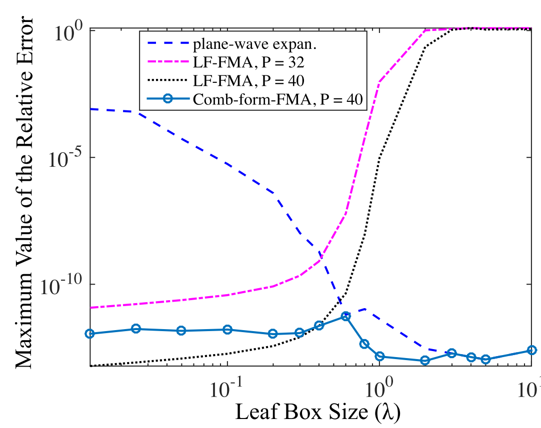


Fig. 8. Maximum relative error for the plane-wave expansion, the LF-FMA, and the Comb-form-FMA. For the Comb-form-FMA, the number of harmonics is 40.

time cost for MVP is shown in Fig. 7, in which the difference between the LF-FMA and the DFT-FMA is not as huge as the time cost in the FMA setup due to the computation of normalization and renormalization, FFT and inverse FFT for each translation.

The error analysis can be found in Fig. 8 with the number of levels as 4. Similar to the error of one-level case (see Fig. 1) in Section II, the plane-wave expansion has the low-frequency breakdown issue, and the LF-FMA is inefficient in the middle-frequency regime. However, the Comb-form-FMA works well for the whole range of

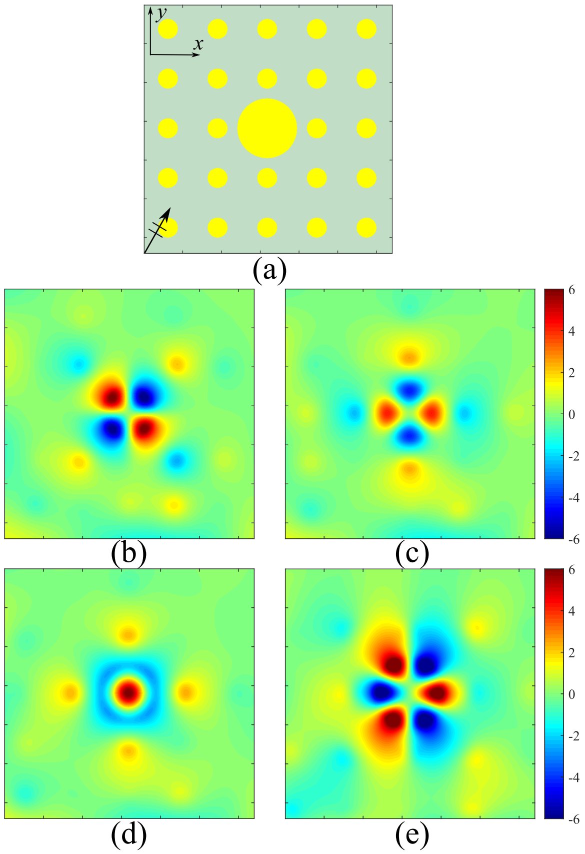


Fig. 9. (a) Photonic crystals with a centered defect. (b) Mode 1: quadrupole (odd–odd). (c) Mode 2: quadrupole (even–even). (d) Mode 3: monopole (second order). (e) Mode 4: hexapole (even–odd).

frequency. Note that, the accuracy of Comb-form-FMA is slightly smaller than the LF-FMA. This is because the machine precision of the inverse FFT cannot recover those extremely small values in the radiation pattern (or the receiving pattern). Overall, the Comb-form-FMA can achieve a wideband algorithm with high accuracy and less computation cost.

### *B. Defect Modes in Photonic Crystals*

The defect modes are the localized states in the bandgap that can be generated by a point defect. To verify that the proposed DFT-FMA works well in the low-frequency regime, we apply it into the VIE to identify the defect modes in 2-D photonic crystals (on $xy$ plane). Here, the TM modes ($\{E_z, H_x, H_y\}$) are studied as an example. All the modes can be excited by an incident plane wave along a nonsymmetric direction of the crystal [16]. We choose the incident angle of the plane wave to be 60° to excite all the modes. The 2-D photonic crystals with a defect at the center can be found in Fig. 9(a), containing GaAs rods with the permittivity of 11.56. The radii of the defect rod and the regular rod are $0.6a$ and $0.2a$, where the lattice length $a$ is 1 $\mu$m. Note that, for our simulation, a supercell approach is adopted. In FMA, the ratio of the box size over the wavelength at the leaf level is set as 0.025 with the resolution of the grids as 0.0025. The number of levels is 7. By choosing the normalized frequency $\omega a/2\pi c$ to be 0.2970, 0.3190, 0.3345, and 0.3916, we can excite quadrupole (odd–odd), quadrupole (even–even), monopole (second order), and hexapole (even–odd) [see Fig. 9(b)–(e) where $E_z$ is plotted]. The "odd/even–odd/even" represents the properties of symmetry to the x- and y-axes. The results match the data from [16] well.

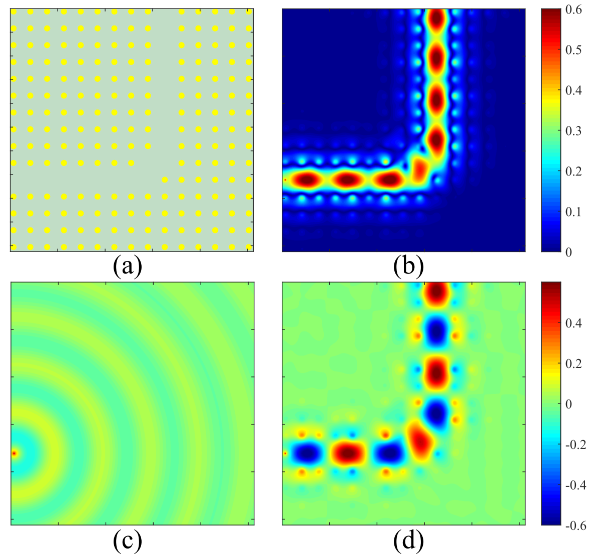


Fig. 10. (a) Photonic waveguide structure. (b) Energy plot. (c) Incident wave by a point source. (d) Total field.

### *C. Photonic Crystal Waveguide*

Now, we study the application for this broadband algorithm in the long wavelength regime. The photonic crystal waveguide with a sharp bend proposed in [17] is studied to observe the high transmission of light. Similarly, the TM modes are analyzed in this scenario. The configuration of the photonic bandgap waveguide is given in Fig. 10(a). The radius of the GaAs rods is $0.18a$, where $a$ is the lattice constant.

In the setup of FMA, the ratio of the box size over the wavelength ($\lambda$) is 0.04 at the leaf level. The number of levels is 8; therefore, the whole computation domain is $5.12\lambda \times 5.12\lambda$. A point source is placed at the center of the input port. The high-efficient transmission can be achieved when the normalized frequency $\omega a/2\pi c$ is set as 0.353. It is consistent with the results in [17]. Fig. 10(b)–(d) shows the energy of the field, the incident field, and the total field in the waveguide, respectively. Combined with previous simulations, we can see that the broadband FMA can work well in both subwavelength and long wavelength problems.

## IV. Conclusion

In this communication, a novel diagonalization for the 2-D FMA is proposed to achieve a highly efficient and accurate broadband FMA. Numerical analyses of the proposed FMA with the applications in photonic crystals demonstrate its performance completely. The derivation, based on Parseval's theorem, provides insights for the 3-D FMA, in which the spherical harmonic transform can be taken as the counterpart of the Fourier transform.

## References

[1] L. Greengard, *The Rapid Evaluation of Potential Fields in Particle Systems*. London, U.K.: MIT Press, 1987.

[2] R. Coifman, V. Rokhlin, and S. Wandzura, "The fast multipole method for the wave equation: A pedestrian prescription," *IEEE Antennas Propag. Mag.*, vol. 35, no. 3, pp. 7–12, Jun. 1993.

[3] W. C. Chew, S. Koc, J. M. Song, C. C. Lu, and E. Michielssen, "A succinct way to diagonalize the translation matrix in three dimensions," *Microw. Opt. Technol. Lett.*, vol. 15, no. 3, pp. 144–147, 1997.

[4] W. C. Chew, J. M. Jin, E. Michielssen, and J. M. Song, *Fast and Efficient Algorithms in Computational Electromagnetics*. Norwood, MA, USA: Artech House, 2001.

[5] L. L. Meng, X. Y. Z. Xiong, T. Xia, and L. J. Jiang, “The error control of mixed-form fast multipole algorithm based on the high-order multipole rotation,” *IEEE Antenn. Wireless Propag. Lett.*, vol. 16, pp. 1655–1658, Jan. 2017.

[6] T. Xia *et al.*, “An enhanced augmented electric-field integral equation formulation for dielectric objects,” *IEEE Trans. Antennas Propag.*, vol. 64, no. 6, pp. 2339–2347, Jun. 2016.

[7] B. Michiels, J. Fostier, I. Bogaert, and D. D. Zutter, “Full-wave simulations of electromagnetic scattering problems with billions of unknowns,” *IEEE Trans. Antennas Propag.*, vol. 63, no. 2, pp. 796–799, Feb. 2015.

[8] I. Bogaert, D. Pissoort, and F. Olyslager, “A normalized plane-wave method for 2D Helmholtz problems,” *Microw. Opt. Technol. Lett.*, vol. 48, no. 2, pp. 237–243, Feb. 2006.

[9] M. Hidayetoğlu, C. Pearson, I. E. Hajj, L. Gürel, W. C. Chew, and W.-M. Hwu, “A fast and massively-parallel inverse solver for multiple-scattering tomographic image reconstruction,” in *Proc. Int. Parallel Distrib. Process. Symp. (IPDPS)*, May 2018, pp. 64–74.

[10] Ö. Ergül and B. Karaosmanoğlu, “Broadband multilevel fast multipole algorithm based on an approximate diagonalization of the Green’s function,” *IEEE Trans. Antennas Propag.*, vol. 63, no. 7, pp. 3035–3041, Jul. 2015.

[11] J. Gu, D. Ding, Z. He, and R. Chen, “A low-frequency EFIE-MLFMA solver based on approximate diagonalization of Green’s function,” *IEEE Trans. Antennas Propag.*, vol. 65, no. 12, pp. 7150–7156, Dec. 2017.

[12] H. Wallén and J. Sarvas, “Translation procedures for broadband MLFMA,” *Prog. Electromagn. Res.*, vol. 55, pp. 47–78, 2005.

[13] I. Bogaert, J. Peeters, and F. Olyslager, “A nondirective plane wave MLFMA stable at low frequencies,” *IEEE Trans. Antennas Propag.*, vol. 56, no. 12, pp. 3752–3767, Dec. 2008.

[14] H. Cheng *et al.*, “A wideband fast multipole method for the Helmholtz equation in three dimensions,” *J. Comput. Phys.*, vol. 216, no. 1, pp. 300–325, Jul. 2006.

[15] A. F. Peterson, S. L. Ray, and R. Mittra, *Computational Methods for Electromagnetics*. New York, NY, USA: IEEE Press, 1998.

[16] S. Guo and S. Albin, “Numerical techniques for excitation and analysis of defect modes in photonic crystals,” *Opt. Express*, vol. 11, no. 9, pp. 1080–1089, May 2003.

[17] A. Mekis, J. C. Chen, I. Kurland, S. Fan, P. R. Villeneuve, and J. D. Joannopoulos, “High transmission through sharp bends in photonic crystal waveguides,” *Phys. Rev. Lett.*, vol. 77, no. 18, pp. 3787–3790, Oct. 1996.